Initial Results on Virtual and Directional Channel Sounding at mmWave

Jose-Maria Molina-García-Pardo, Davy P. Gaillot, M. T. Martinez-Ingles,

Antonio Mateo and Juan Pascual-García

Josemaria.molina@upct.es, davy.gaillot@univ-lille.fr, mteresa.martinez@cud.upct.es, antonio.mateo@upct.es, juan.pascual@upct.es

(1) Dpto. de Tecnologías de la Información y Comunicaciones, Universidad Politécnica de Cartagena, Cartagena 30202, España

(2) University of Lille, CNRS, UMR 8520 - IEMN Lille .

(3) Centro Universitario de la Defensa, Ministerio de Defensa, San Javier, España

***Abstract*— This work presents preliminary results on a measurement campaign at mmwave between 26 and 40 GHz in an indoor environment in line-of-sight conditions. 2D-virtual arrays and 3D-directional sounding were tested in the same identical positions to investigate the accuracy of both approaches by comparing the directional characteristics of the double directional radio channel. The radio channels and corresponding characteristics were also simulated with an in-house 3D ray tracer. The results show that both approaches are different by nature, due to the fact that different antennas are used in each approach. URA and 3D rotor share the same large-scale characteristics. The capacity of the 3D rotor to sound the channel in the elevation plane is better than that of the more complex planar URA due to its limited aperture and the use of an omnidirectional antenna. This comes at the expense of longer measurements as the number of positions is much larger.**

***Index Terms*—Propagation, Channel Sounding, mmwave, virtual array, beamformer, Rimax.**

I. Introduction

Millimeter wave (mmwave) communications is considered to be a promising technology for already-deployed 5G networks as well as for future 6G networks [1,2]. Main reasons are, firstly because in mmWave frequencies from 6 GHz up to 300 GHz, there are many unlicensed bands – the available spectrum is abundant. Secondly, the absolute bandwidth at mmWave frequencies is much larger than that at the lower microwave frequencies under the same relative bandwidth.

However, the use of mmwave frequencies leads to unaffordable path losses with omnidirectional antennas mainly due to the very small antenna apertures. To overcome the large free-space path loss of the radiated waves at mmwave frequencies, beamforming techniques are widely employed in 5G/6G wireless systems for effectively focusing the radiated energy into the targeted directions.

Indeed, one of the most promising techniques in 5G/6G is massive MIMO [3,4]. It is based on a large number of radiating elements at the transmitting side paired with a number of active users, which permits the use of simple linear precoders and increases the overall spectrum efficiency [5].

Direction-of-arrival (DOA) estimation is the preliminary stage of communication, localization, and sensing [6]. There are many approaches such as using directional antennas [7] or by estimating with high resolution algorithms, being one of the most accurate one Rimax [8].

The objective of this paper is to channel sound and channel model a well-known reference indoor scenario [9], by means of i) deterministic tools, ii) measurements with virtual arrays and omni antennas, and iii) a 3D rotor positioner with directive antennas. Then, all approaches are compared to verify the accuracy and benefits of each approach. The capacity of the 3D rotor to sound the channel in the elevation plane is better than that of the more complex planar URA due to its limited aperture and the use of an omnidirectional antenna. This comes at the expense of longer measurements as the number of positions is much larger.

The paper is organized as follows. Section II describes the scenario and the channel sounder. Section III presents the simulation tool and preliminary results are presented in section IV. Section V sums up the work with the main conclusions.

II. Scenario and Channel Sounder

Measurements were carried out in a laboratory room at the *Universidad Politécnica de Cartagena*, with a volume of 8 x 4.8 x 3.5 m^3. Figure 1 shows a scheme of the laboratory with the positions selected for the transmitters (Tx 1 to 6) and one receiver (Rx). The lab is furnished with desks, chairs, shelves, and closets, and is equipped with electronic devices such as computers. Table I shows exact positions for each transmitter location with Tx – Rx distance values ranging between 1 and 5 meters. A, B and C in Fig. 1are distances to walls.

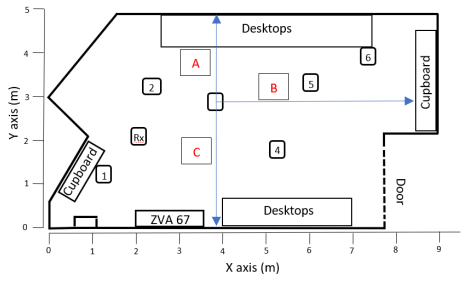

a)

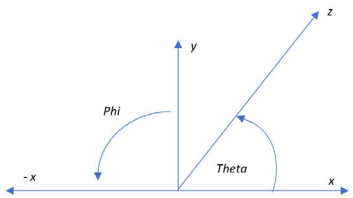

b)

Figure 1: a) Top view and positions of Tx and Rx in the room and b) Theta/Phi angle definition for results representation

Table I: Position of the transmitters and the receiver

Position	A (m)	B (m)	C (m)	Tx-Rx Distance (m)
1	3.598	6.644	1.230	1.118
2	1.769	6.110	3.042	1.007
3	2.006	4.651	2.589	1.877
4	3.153	2.317	1.405	3.322
5	1.613	2.400	2.466	3.733
6	0.928	1.098	3.625	5.200
Rx	2.867	5.770	1.952	

All measurements have been performed using a commercial vector network analyzer (VNA) (Rohde and Schwarz ZVA 10 MHz - 67 GHz). To reach all locations in the room, an additional radio over fiber (RoF) link (EMCORE, Optiva OTS-2, 40 GHz) has been used. The number of frequency points is 1024, and the intermediate frequency is 100 Hz. The measured frequency band is in the 26 - 40 GHz range.

The transmitted antenna is located at 6 positions whereas the Rx antenna is fixed. In the measurements, the Tx and Rx height was always set to 1.301 m. In the case of the Tx antenna, an omni antenna was used. For the Rx antenna, two configurations have been considered.

- Omni antenna. Ultra-wideband Omnidirectional Antennas (STEATITE Q-PAR ANTENNAS, 0.8-40 GHz). The antenna in Rx is moved along a 2D URA (Uniform Rectangular Array (URA)) forming a planar 10 x 10 virtual array with 3 mm in each dimension (wavelength at 40 GHz is 7.5 mm). The Tx antenna is the same.
- Horn antenna. Steatite Q-PAR QSH-26-40-K-20, with 17.7 to 20.9 dBi gain, and 3dB beam width from 14.5 to 22.5 degrees in the 26 – 40 GHz frequency band. It is orientated with a 3D rotor, scanning full azimuth every 4 degrees (91 positions), and elevation from - 64 degrees to + 48 degrees (28 positions with zero being the broadside direction).

Figure 2 presents the two types of antennas used in the measurement setup.

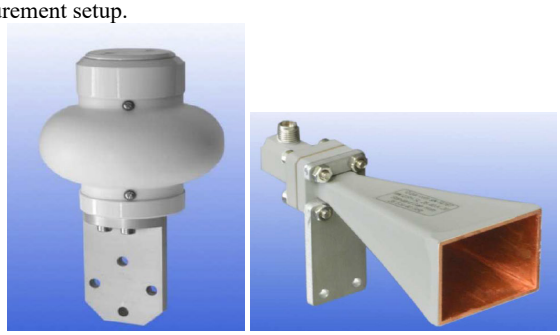

Figure 2: Photos of the omni antenna and directional antenna.

Figures 3 and 4 show both approaches for Rx position 1: URA array using the omni antenna (Fig. 3) and directional horn antenna orientated with a 3D rotor (Fig. 4).

III. Simulations

In addition to the measurements, the double directional radio channels were simulated using a 3D ray-tracing tool (RT) programmed by our research group in MATLAB. In this work, only reflections and the direct ray were included in the simulations. Due to memory and time limitations, up to three order reflections were considered as the results show this number is enough to simulate the main reflections in the environment. To achieve a good accuracy the measured radiating pattern of the antennas were included in all simulations. Further propagation mechanisms such as diffraction and diffusion will be included in a future work.

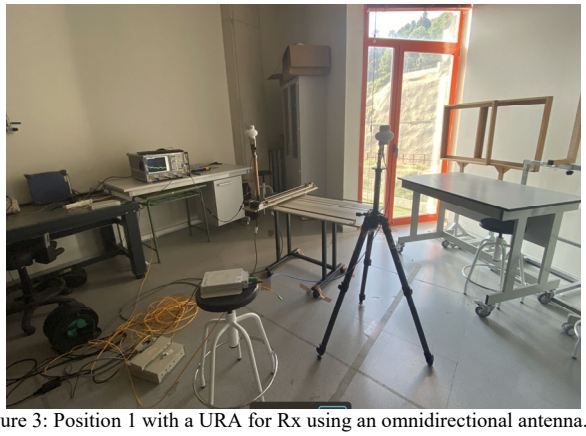

Figure 3: Position 1 with a URA for Rx using an omnidirectional antenna.

Figure 4: Position 1 with the 3D rotor for Rx using a horn antenna.

IV. Results

In a first step, the measured averaged Power Delay Profile (PDP) are compared between both measurement approaches. As an example, for position 6, Fig. 5 shows the averaged PDP over the 10 x 10 URA (blue curve) and the 3D Rotor (red curve). In the case of the URA, it has been averaged over 100 positions (10 x 10). For the 3D rotor, 2548 positions were used (91 x 28). That explains the different noise levels with a difference of about 14 dB ($10\log_{10}(91 \cdot 28 - 10 \cdot 10)=14$ dB).

It can be observed a sufficient dynamic range in the measurements with the main multipath components (MPC) occurring within 6- and 14-meters time of flight for this position.

The different MPC gain values are due to the gain of the antennas, being the elevation plane different of the omni antenna compared to the horn antenna. For example, the omni antenna has a 3dB beamwidth in the measured frequency range of about 30 degrees, whereas the horn antenna scans from - 64 degrees to + 48 degrees using the maximum gain of the horn antenna, attenuating other components.

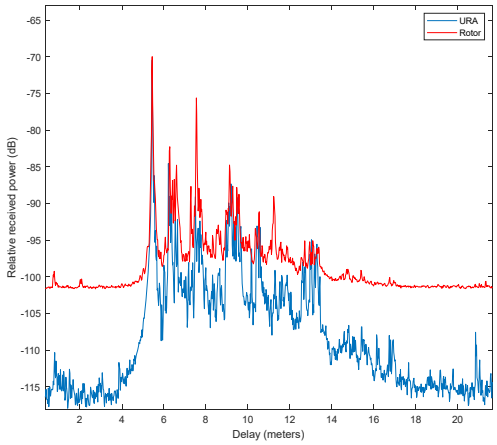

Figure 5: PDP using all data for position Tx6.

Figures 6 and 7 present the averaged power angular-delay profile along the elevation (Theta) and azimuth planes (Phi) using the 3D rotor for position 6, respectively.

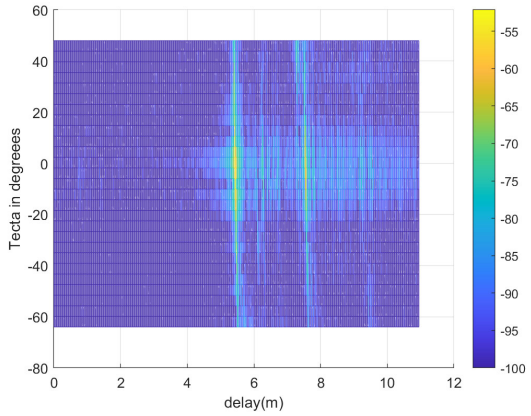

Figure 6: Averaged power Angular-Delay Profile in the elevation plane (Theta) for Position 6 using the 3D rotor.

In both cases the LoS component can be identified, corresponding to a theta value of 0 degree, and phi value of 290 degrees. The CIR (Complex Impulse Response) which corresponds to that orientation of the horn antenna is shown in Fig. 8. The LoS component is detected at 5.42m that is 20 cm larger than the measured distance. This is because the electrical length of antennas from the SMA connector is not taken into account in the calibration process.

In a subsequent step, the URA data has been analysed using the high-resolution parametric estimator Rimax without the estimation of the dense multipath component using a reduced array subset of 5 x 5 [8]. For this analysis, different bandwidths were used since the algorithm is narrow band in the spatial domain but wide band in the delay domain. Note that at this point of the analysis the antennas were not de-embedded in the estimator. Figure 9 presents the received power, angle of arrival in the azimuth and elevation domains of the estimated MPC as a function of the delay (in ns). The data is superimposed with the MPC extracted as maxima from the 3D rotor data. It can be qualitatively observed that the MPC are similarly clustered in the azimuth domain. On the other hand, it appears greater MPC with greater elevation angles using the URA data. This is because the pattern of the omnidirectional antenna is not included in the estimator despite not being omni in the elevation plane.

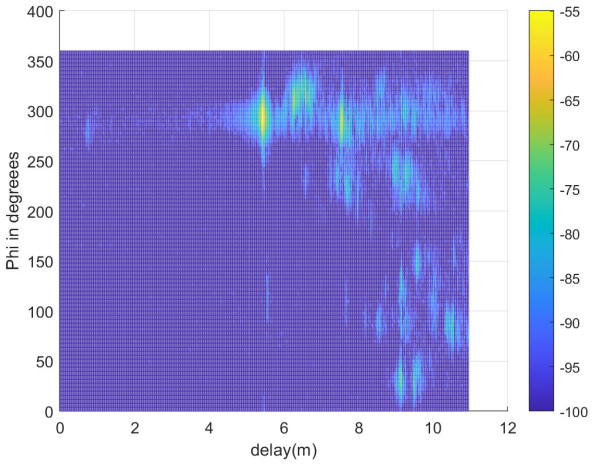

Figure 7: Averaged power Angular-Delay Profile in the azimuth plane (Phi) for Position 6 using the 3D rotor.

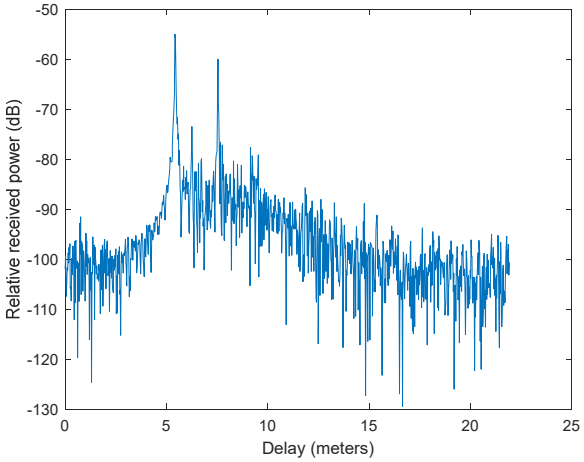

Figure 8: CIR corresponding to the 3D rotor pointing toward the emitting antenna for position 6 (Theta = 0 degree and Phi = 290 degrees).

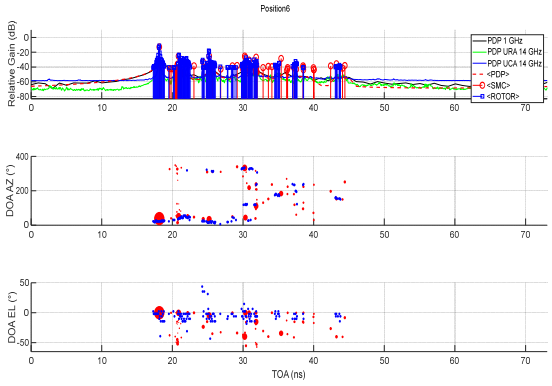

Figure 9: MPC extraction using Rimax with the URA for Position 6 compared with the MPC extracted from the 3D rotor as maxima.

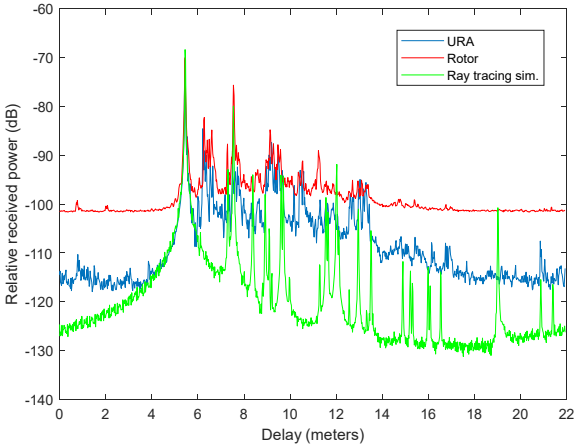

Figure 10: PDP using all data for position Tx6 adding simulations.

Figure 10 shows same result as Fig. 5 including simulations using the RT tool. Some of the main components have been identified. Firstly, at 6 meters a first order reflection coming from the floor is identified, this reflection has low power because the small value of the antenna gain. At 7.5 meters another first order reflection with high power, coming from one of the walls, is present. Between 9.5 and 9.7 meters some relevant reflections are present: the first one is a first order reflection and the other two correspond to second order reflections. Between 11.5 and 12 meters other important second order reflections have been identified. The three order reflections become relevant from a path distance around 12 meters, where first and second order reflections are absent.

Finally, the RMS delay and angular spreads have been computed for the 3D rotor, URA and ray tracing simulations and are presented in Fig. 11. The MPC were extracted from the RT channels using Rimax for the sake of the comparison. Overall, the spreads results are very similar across the delay, azimuth and elevation domains. It is simply noted smaller elevation spread values for the ray-traced radio channels using the URA. This is because the RT channels include the antenna patterns whereas it is not de-embedded in the estimator; this fact produces in the RT simulations an extra attenuation in the components corresponding to elevation angles different from 90º, where the maximum gain is achieved; in other words, only those components with elevation angles equal to 90º have powers above the threshold. In addition, it appears the 2 first positions (1 meter Tx – Rx distance) exhibit lower delay and azimuth spreads for the 3D rotor and estimated MPC from the RT channels. For the latter, lower delay spreads are also obtained for longer distances (positions 5 and 6). It can be safely concluded from the preliminary analysis that the URA and 3D rotor share the same large-scale characteristics. The capacity of the 3D rotor to sound the channel in the elevation plane is better than that of the more complex planar URA due to its limited aperture and the use of an omnidirectional antenna. This comes at the expense of longer measurements as the number of positions is much larger.

V. Conclusion

In this work, preliminary results on a measurement campaign at mmwave (26 - 40 GHz) have been presented in an indoor scenario with a LoS. 2D-virtual arrays and 3D-directional sounding have been tested in the same identical positions, to investigate the accuracy of both approaches to extract the directional characteristics of the double directional radio channel, also being compared to 3D ray tracing simulations. Results show that main MPC characteristics are extracted, which the antenna patterns influence quite a lot in determine the main components.

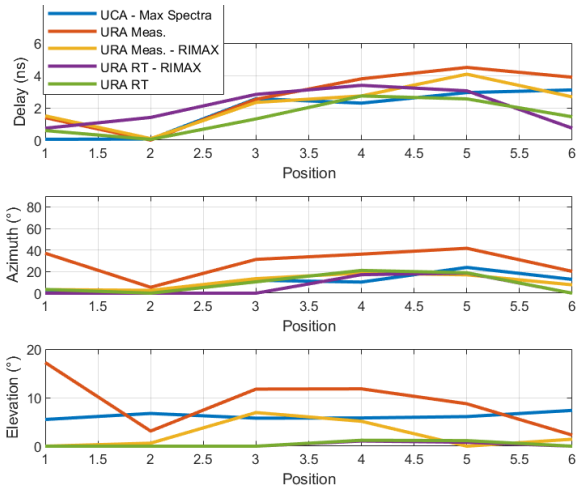

Figure 11: Delay, Azimuth and Elevation spreads for the 6 positions.

Acknowledgment

Grant PID2022-136869NB-C32 funded by MCIN/AEI/10.13039/501100011033 and, as appropriate, by “ERDF A way of making Europe”, by the “European Union” or by the “European Union NextGenerationEU/PRTR”.

References

[1] W. Hong et al., "The Role of Millimeter-Wave Technologies in 5G/6G Wireless Communications," in IEEE Journal of Microwaves, vol. 1, no. 1, pp. 101-122, Jan. 2021, doi: 10.1109/JMW.2020.3035541.

[2] H. Tataria, M. Shafi, A. F. Molisch, M. Dohler, H. Sjöland and F. Tufvesson, "6G Wireless Systems: Vision, Requirements, Challenges, Insights, and Opportunities," in Proceedings of the IEEE, vol. 109, no. 7, pp. 1166-1199, July 2021, doi: 10.1109/JPROC.2021.3061701.

[3] F. A. Pereira de Figueiredo, "An Overview of Massive MIMO for 5G and 6G," in IEEE Latin America Transactions, vol. 20, no. 6, pp. 931-940, June 2022, doi: 10.1109/TLA.2022.9757375.

[4] Emil Björnson; Jakob Hoydis; Luca Sanguinetti, Massive MIMO Networks: Spectral, Energy, and Hardware Efficiency , now, 2017.

[5] T. L. Marzetta, "Noncooperative Cellular Wireless with Unlimited Numbers of Base Station Antennas," in IEEE Transactions on Wireless Communications, vol. 9, no. 11, pp. 3590-3600, November 2010, doi: 10.1109/TWC.2010.092810.091092.

[6] Ruan, N.; Wang, H.; Wen, F.; Shi, J. DOA Estimation in B5G/6G: Trends and Challenges. Sensors 2022, 22, 5125. https://doi.org/10.3390/s22145125

[7] C. -X. Wang, J. Bian, J. Sun, W. Zhang and M. Zhang, "A Survey of 5G Channel Measurements and Models," in IEEE Communications Surveys & Tutorials, vol. 20, no. 4, pp. 3142-3168, Fourthquarter 2018, doi: 10.1109/COMST.2018.2862141.

[8] A. Richter, “Estimation of radio channel parameters: Models and algorithms,” Ph.D. dissertation, Fakültat für Elektrotechnik und Informationstechnik, Technische Universität Ilmenau, Ilmenau, Germany, 2005.

[9] M. -T. Martinez-Ingles, D. P. Gaillot, J. Pascual-Garcia, J. -M. Molina-Garcia-Pardo, M. Lienard and J. -V. Rodríguez, "Deterministic and Experimental Indoor mmW Channel Modeling," in IEEE Antennas and Wireless Propagation Letters, vol. 13, pp. 1047-1050, 2014, doi: 10.1109/LAWP.2014.2327054..